BULLETIN OF THE POLISH ACADEMY OF SCIENCES
TECHNICAL SCIENCES, Vol. 67, No. 3, 2019
DOI: 10.24425/bpasts.2019.129658

Control and optimisation of photovoltaic water pumping system using sliding mode

L. ZAROUR[1]*, K. ABED[1], M. HACIL[1], and A. BORNI[2]

[1] Université Frères Mentouri Constantine, 25000, Departement d'électrotechnique, Laboratoire électrotechnique Constantine *LEC*, Algeria
[2] Unité de Recherche Appliquée en Energies Renouvelables, URAER, CDER, 47133, Ghardaïa, Algeria

Abstract. A sliding mode controller for the photovoltaic pumping system has been proposed in this paper. This system is composed of a photovoltaic generator supplying a three-phase permanent magnet synchronous motor coupled to a centrifugal pump through a three-phase voltage inverter. The objective of this study is to minimise the number of regulators and apply the sliding mode control by exploiting the specification of the field oriented control scheme (FOC). The first regulator is used to force the photovoltaic generator to operate at the maximum power point, while the second is used to provide the field oriented control to improve the system performance.The whole system is analysed and its mathematical model is done. Matlab is used to validate the performance and robustness of the proposed control strategy.

Key words: photovoltaic pumping system modelling, optimization, maximum power point, MPPT, sliding mode control.

1. Introduction

Algeria is one of the sunniest countries in the word. It receives an average of 10 hours of sunlight per day, which is equivalent to 8 kWh/m^2, and approximately equivalent to one litre of gasoline [4]. This advantage makes the production of electricity from the solar energy very interesting and important to Algerian localities, especially for isolated sites and remote rural areas far from electrical network, and in particular for pumping drinking water systems.

The first studies of photovoltaic pumping systems are based on different types of DC motors coupled directly with photovoltaic generator. In addition, the development of power electronics allows the use of different type of DC-DC converters to solve the adaptation problem and increases the efficiency of the system [1]. However, the maintenance presents difficulties, in particular at the level of hostile sites and deep layers.

The development of magnetic materials technology has permitted the exploitation of PMSM. These last are more efficient and give best performance and high adaptability as compared to the induction motors [6–8].

The work is carried out using two converters: one is the DC-DC for the adaptation and the other is the DC-AC for the conversion [1, 10, 11, 13]. These systems work well but they are costly. This has led researchers to implement systems based only on DC-AC converter [5, 12]. But the difficulty remains at the level of the inverter control. The majority of the work done in this direction is focused on estimating one of two magnitudes: the optimum motor speed or the optimum voltage of the PV generator that depend on the efficiency of the system [6, 15, 16]. This approach remains approximate because of the very significant variation in the efficiency of the system, witch depends on the different parameters of the system.

The photovoltaic pumping system is shown in Fig. 1. It consists of a PV generator, input capacitor, three-phase voltage inverter controlled by PWM technique and a PMSM which is coupled to a centrifugal pump. The PV generator is controlled in order to operate at the maximum power point for weather situations.

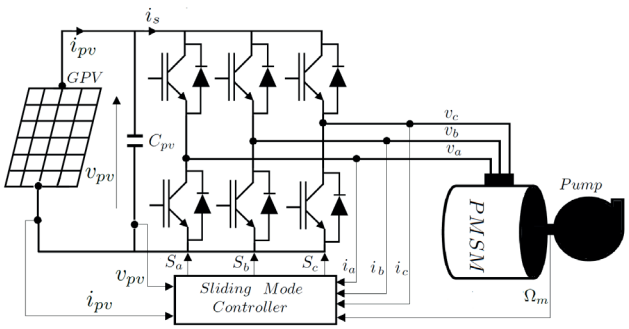

Fig. 1. Synoptic scheme of photovoltaic system

The system control requires a solution that takes into account the climate change which is random and the non-linearity of the mathematical model of the entire system. To deal with this problem, the PMSM model are adopted in Park coordinate system and the field oriented control is applied to it in order to obtain an equivalent structure of the separately ex-

*e-mail: laidzarour@hotmail.fr

Manuscript submitted 2018-03-04, revised 2018-05-14, initially accepted for publication 2018-07-14, published in June 2019.

cited DC motor [9, 18, 20, 21, 23, 24]. Despite the simplicity of the proposed system, the variation of the parameters remains and affects the performance of the system. For this, the sliding mode control SMC and FOC are used [2]. With this last, the decoupling between the direct and quadratic component of the PMSM current allows each component to be controlled separately. The direct component is used to control the excitation and the quadratic component to extract the maximum power generated by the PV generator. For this, only two surfaces of sliding mode are implanted: one depends on the (i_d) component and the second depends on the variation of the PV generator power $(\partial P_{pv}/\partial i_p v \cong 0)$. From these two sliding surfaces, the functions of the inverter switches are obtained in dq axis (S_d, S_q) using Park inverse transformation with the abc coordinate. These are used to attack the arms of the inverter.

The mathematical modelling of the system has been done and the simulation has been performed using Matlab.

2. Proposed system modelling

2.1. PV generator model. Equivalent electrical model of the PV generator is depicted in Fig. 2. It consists of a photo-current source, a diode which represents the P-N junction of the generator and a series resistance.

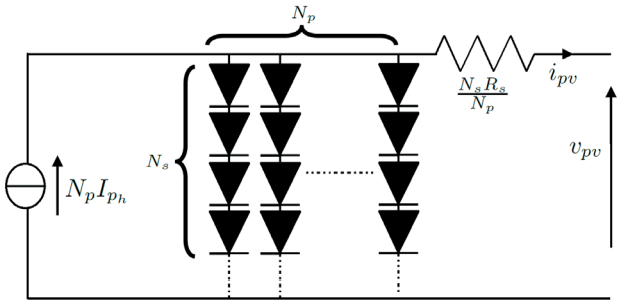

Fig. 2. Electrically equivalent circuit of PV generator

The relation between the voltage and current delivered by the PV generator is described as follows [3]:

$$i_{pv} = N_p I_{p_h} - N_p I_o \left[\exp\left(\frac{q}{K\gamma T}\right)\left(\frac{V_{pv}}{N_s} + \frac{R_s i_{pv}}{N_p}\right) - 1\right], \quad (1)$$

with: i_{pv}, I_{ph} and I_o represents respectively: the current of the PV generator, the photo-current and the diode current inverse saturation. γ is the diode quality factor, $K = 1.38 \cdot 10^{23}$ J/°K is the Boltzmann constant, $q = 1.6 \cdot 10^{-19}$ C is the electron charge, T is the ambient temperature in Kelvin. R_s is the series resistance and v_{pv} is the voltage of the PV generator; N_p represents the number of parallel module and each module is composed of N_s cells connected in series.

Knowing that [3]:

$$I_{ph} = \frac{G}{G_{ref}}\left(I_{ph-ref} + \mu_{Isc}(T - T_{ref})\right), \quad (2)$$

$$I_o = I_{o-ref}[T/T_{ref}]^3 \exp\left[\frac{q\varepsilon_G}{K\gamma}\left(\frac{1}{T_{ref}} - \frac{1}{T}\right)\right], \quad (3)$$

where: I_{ph-ref}, I_{o-ref} are photo-current and inverse saturation current respectively at the reference condition, ε_G is the band-gap energy of the semiconductor.

The type of the PV generator used in this study is: BP SX 150S PV module, and its characteristics are illustrated in Fig. 3 and Table 1.

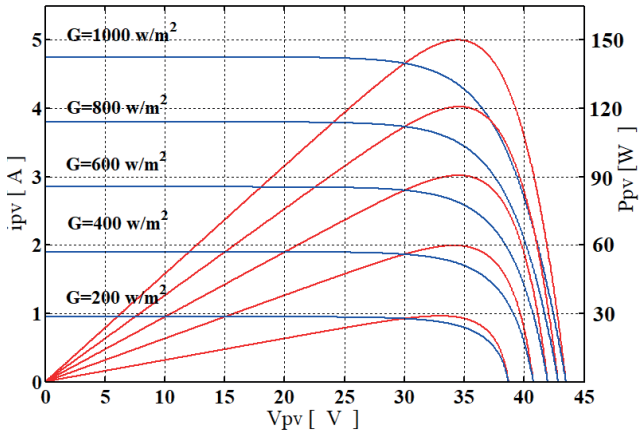

Fig. 3. $i_{pv} - v_{pv}$, $P_{pv} - v_{pv}$ characteristics at $T = 25$°C

Table 1
BP SX 150S PV characteristics

Parameters	Value
Maximum power P_{Max}	150 W
Maximum power current (I_{mp})	4.35 A
Maximum power voltage (V_{mp})	34.5 V
Open-circuit voltage (V_{oc})	43.5 V
Short circuit current (I_{sc})	4.75 A
Voltage temperature coefficient (μ_{Voc})	$-(160 \pm 20)$ mV/°C
Current temperature coefficient (μ_{Isc})	$0.065 \pm 0.015\%$/°C

2.2. Photovoltaic pumping system model. In the reference dq oriented to the rotor, an electrical equation model of the PMSM (with smooth air gap $L_d = L_q = L_s$) coupled to PV generator through a voltage inverter can be formulated as:

$$C_{pv}\frac{dv_{pv}}{dt} = i_{pv} - (S_d i_d + S_q i_q), \quad (4)$$

$$L_s\frac{di_d}{dt} = v_d - R_a i_d + p\Omega_m i_q, \qquad v_d = S_d v_{pv}, \quad (5)$$

$$L_s\frac{di_q}{dt} = v_q - R_a i_q - p\Omega_m i_d - p\phi_m\Omega_m, \qquad v_q = S_q v_{pv}, \quad (6)$$

with: R_a is the stator winding resistance, L_s stator winding inductance, ϕ_m is the permanent magnet rotor flux (Wb), Ω_m is the rotational speed (rad/s), C_{pv} is the DC link capacitor, i_d, i_q, v_d, v_q, S_d, S_q are respectively, the dq components of the stator current voltage and switch control signals.

The transformation matrix $\left[K_{abc}^{dqo}\right]$ is given by:

$$K_{abc}^{dqo} = \frac{2}{3}\begin{bmatrix} \cos\theta & \cos\left(\theta-\frac{2\pi}{3}\right) & \cos\left(\theta+\frac{2\pi}{3}\right) \\ \sin\theta & \sin\left(\theta-\frac{2\pi}{3}\right) & \sin\left(\theta+\frac{2\pi}{3}\right) \\ \frac{1}{2} & \frac{1}{2} & \frac{1}{2} \end{bmatrix}. \quad (7)$$

In dq transformation, it can be written:

$$[S_{dqo}] = [K_{abc}^{dqo}][S_{abc}], \qquad [i_{dqo}] = [K_{abc}^{dqo}][i_{abc}],$$

$$[v_{dqo}] = [K_{abc}^{dqo}][v_{abc}].$$

The electromagnetic torque developed by the PMSM coupled to a centrifugal pump is given by:

$$T_e = p\phi_m i_q = J_m\frac{d\Omega_m}{dt} + k_v\cdot\Omega_m + K_r\cdot\Omega_m^2, \quad (8)$$

$$\frac{d\theta_m}{dt} = p\Omega_m, \quad (9)$$

with θ_m is the position angle; J_m, k_v, k_r, p, are respectively the moment inertia of group motor-pump [kg·m^2], the friction coefficient, the centrifugal pump constant and the pole pairs number.

3. Design of the sliding mode controller

3.1. Theory of sliding mode technique. Let the non-linear space-state model of the following structure:

$$\dot{x} = f(x,t) + g(x)u(t), \qquad x\in R^n, \quad u\in R, \quad (10)$$

where x is a vector function, $f(x)$ and $g(x)$ represents uncertain smooth functions, and u is a command vector.

The sliding surface is described as follows [2]:

$$\sigma(x) = x_{ref} - x \quad (11)$$

and the derivation of formula (10):

$$\dot{\sigma}(x) = \frac{\partial\sigma(x)}{\partial x}\frac{\partial x}{\partial t} = \frac{\partial\sigma(x)}{\partial x}(f(x,t)+g(x)u). \quad (12)$$

The control law $u(t)$ has decomposed at two components [2]:

$$u(t) = u_{eq}(t) + u_n(t), \quad (13)$$

where u_{eq} represent the equivalent control input, it serves to maintain the variable to be controlled on the sliding surface $(\sigma(x)=0)$, this component is obtained from the invariance condition $(\dot{\sigma}(x)=0)$ [2]. By substituting Eq. (13) in Eq. (12) and take into consideration with this the last condition allows to deduce the command u_{eq}.

$$u_{eq} = \left[\frac{\partial\sigma(x)}{\partial x}g(x)\right]^{-1}\left[\frac{\partial\sigma(x)}{\partial x}f(x)\right] \quad (14)$$

with $\left(\frac{\partial\sigma(x)}{\partial x}g(x)\right)\neq 0$.

The component u_n is a switching input that controls the convergence condition $(\sigma(x)\cdot\dot{\sigma}(x)<0)$.

For the reasons of simplicity the u_n is described as:

$$u_n = K_n Sign(\sigma(x)) \quad (15)$$

Sign is a relay function, K_n is a positive constant representing the gain of the discontinuous control.

3.2. MPPT controller design. The first control objective is to extract the PV generator to operate at its maximum power point MPPT (see Fig. 4).

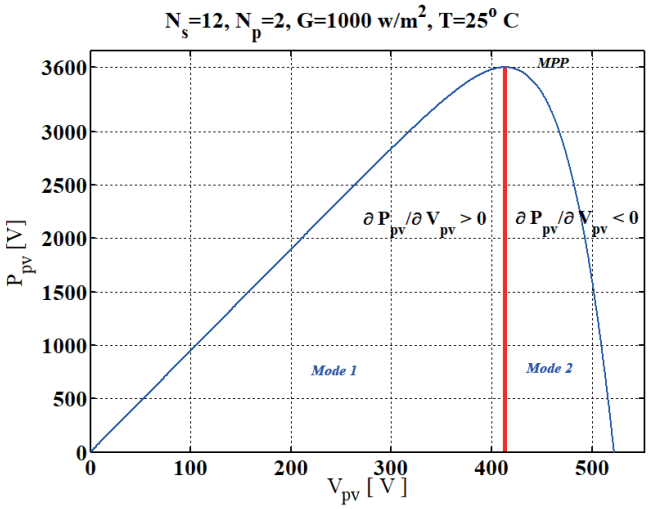

Fig. 4. Moving the operating point on the $P_{pv}-v_{pv}$

From Fig. 4, we can take the expression of the sliding surface as follows:

$$\sigma(v_{pv}) = v_{pv}\frac{\partial i_{pv}}{\partial v_{pv}} + i_{pv} \cong 0. \quad (16)$$

Then the derivative from this surface is:

$$\dot{\sigma}(v_{pv}) = \left(\frac{\partial^2 i_{pv}}{\partial^2 v_{pv}} + 2\frac{\partial i_{pv}}{\partial v_{pv}}\right)\frac{\partial v_{pv}}{\partial t}. \quad (17)$$

The strategy of the vector control of the PMSM consists of orienting the d axis of the dq axis to obtain the component of the direct current equal to zero $(i_d = 0)$, (Fig. 5).

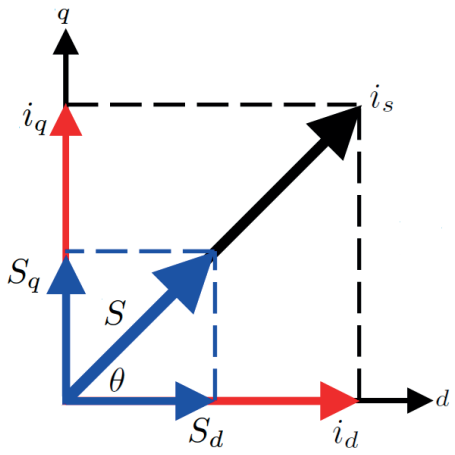

Fig. 5. Diagram of components of S_d and S_q in dq axis (FOC)

From this strategy, Eq. (4) can be written as:

$$C_{pv}\frac{dv_{pv}}{dt} = i_{pv} - S_q i_q \,. \tag{18}$$

The quadratic switch control signal S_q can be expressed as a function of equivalent quadratic signal S_{q_eq} and non-linear quadratic commutation signal S_{q_n} as follows:

$$S_q = S_{q\_eq} + S_{q\_n} \,. \tag{19}$$

Substituting Eq. (17) and Eq. (18) into Eq. (16), and taking into account the convergence conditions ($\dot{\sigma}(v_{pv}) = 0$), we get:

$$S_{q\_eq} = \frac{i_{pv}}{i_L} \,. \tag{20}$$

The relationship between the non-linear quadratic commutation input signal S_{q-n} and the operating point position on the $P_{pv} - v_{pv}$ curve can be expressed by:

$$S_{q-n} = \begin{cases} 0 & \text{si } \sigma(v_{pv}) \geq 0, \\ 1 & \text{si } \sigma(v_{pv}) < 0. \end{cases} \tag{21}$$

3.3. Second sliding surface. The sliding surface of the direct current regulation i_d:

$$\sigma(i_d) = i_{d\_ref} - i_d \,, \tag{22}$$

$$\dot{\sigma}(i_d) = \dot{i}_{d\_ref} - \dot{i}_d \,. \tag{23}$$

We applied the vector control strategy, and replacing Eq. (5) in equation Eq. (23), we obtain:

$$\dot{\sigma}(i_d) = \dot{i}_{d\_ref} - (v_d - R_a i_d + p\Omega_m i_q) \,. \tag{24}$$

The component of the reference direct voltage v_{d_ref} of the PMSM is described by:

$$v_{d\_ref} = v_{d\_eq-ref} + v_{d\_n\_ref} \,. \tag{25}$$

By replacing Eq. (24) in Eq. (23) and taking into account the convergence conditions $\dot{\sigma}(i_d) = 0$, the expression of the equivalent reference direct voltage is

$$v_{d\_eq-ref} = R_a i_d + p\omega_m i_q + L_s \dot{i}_{d\_ref} \tag{26}$$

we deduce:

$$\begin{aligned} S_{d-eq} &= \frac{v_{d\_eq-ref}}{v_{pv}} \\ &= \frac{R_a i_d + p\omega_m i_q + L_s \dot{i}_{d\_ref}}{v_{pv}} \,. \end{aligned} \tag{27}$$

The non-linear component of the direct switch equation can be chosen as follows:

$$S_{q-n} = k_d \cdot Sign(i_d). \tag{28}$$

Fig. 6 shows the synoptic of the overall controller configuration of the proposed system.

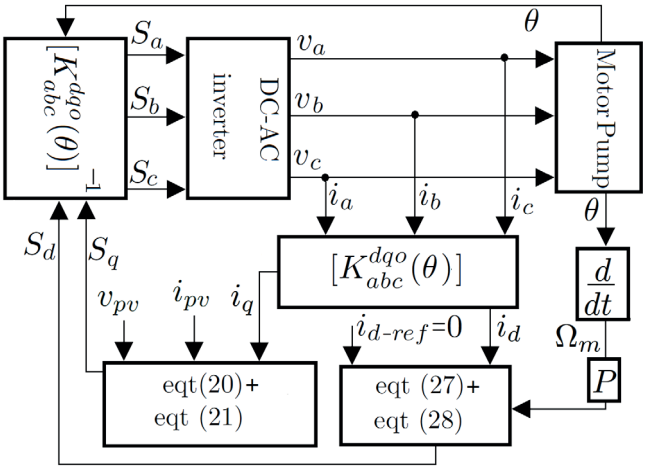

Fig. 6. Block diagram of the proposed controller

a – Condition of existence ($\sigma(v_{pv})\dot{\sigma}(v_{pv}) < 0$)**:** If we neglect the effect of resistance (R_s), and substituting Eq. (6) into Eq. (15), we deduce

$$\begin{aligned} \sigma(v_{pv}) &= \frac{\partial P_{pv}}{\partial v_{pv}} \\ &= (I_L + I_o) - I_o\left(1 + \frac{qv_{pv}}{K\gamma T}\right)\exp\left(\frac{qv_{pv}}{K\gamma T}\right) \end{aligned} \tag{29}$$

and

$$\begin{aligned} \frac{\partial \sigma_{pv}}{\partial t} = -I_o &\left(\left(\frac{q}{K\gamma T}\right)\exp\left(\frac{qv_{pv}}{K\gamma T}\right) + \left(1 + \frac{qv_{pv}}{K\gamma T}\right)\right. \\ &\left.\left(\frac{q}{K\gamma T}\right)\left[\exp\left(\frac{qv_{pv}}{K\gamma T}\right)\right]\right)\frac{\partial v_{pv}}{\partial t} \,. \end{aligned} \tag{30}$$

The system is operating in state **Mode1** the switch quadratic function $(S_{q-n} = 0)$, and v_{pv} is increasing.

$$\frac{\partial v_{pv}}{\partial t} > 0 \tag{31}$$

By replacing in the expression Eq. (30), he comes $\dot{\sigma}(v_{pv}) > 0$:
From where: $(\sigma(v_{pv})\dot{\sigma}(v_{pv}) < 0)$

When $\sigma(v_{pv}) < 0$
The system is operating in state **Mode2** the switch quadratic function $(S_{q-n} = 1)$, and v_{pv} is decreasing

$$\frac{\partial v_{pv}}{\partial t} < 0. \tag{32}$$

By replacing in the expression Eq. (30), we obtain $\dot{\sigma}(v_{pv}) < 0$:
From where: $(\sigma(v_{pv})\dot{\sigma}(v_{pv}) < 0)$
It is concluded that the system is asymptotically stable.

b – Condition of existence $(\sigma(i_d)\dot{\sigma}(i_d) < 0)$**:**
Can be determined as follows:

$$\sigma(i_d) \cdot \dot{\sigma}(i_d) = -\frac{k_d}{L_s}\left(i_{d\_ref} - i_d\right) Sign(i_{d\_ref} - i_d). \tag{33}$$

Whatever the sign of surface $\sigma(i_d)$, Eq. (32) always yields less than zero.

4. System simulation and discussion

The proposed system is simulated in the Matlab environment, and the obtained results are illustrated in Fig. 8.

The PV generator is composed of two parallel chains of twelve panels $(N_s = 12, N_p = 2)$ in order to provide the power which will be absorbed by the PMSM of (3.6 kW) at the reference conditions ($G = 1000$ W/m^2, $T = 25°$C).

To test the performance and the robustness of the proposed control, we apply every two seconds a variation which concerns both the irradiation and the temperature as illustrated in the results in Fig. 7

MPPT controller by SMC forces the PV generator to operate at the maximum power point despite weather changes (Fig. 8 a, b).

This efficiency is observed both at the voltage level and the PV generator power that are well regulated and follow their references after a response time $t = 18$ ms.

The FOC by the MGC technique verifies the decoupling between the direct and quadratic component of the current where (iq) follows the PV generator power variation and (i_d) is equal to zero during all the functioning phases (see Fig. 8 c). In addition, this setting gives very good tracking results without an overshoot for all the magnitudes except for the quadratic component which stabilizes after a time of 18 ms with an overshoot of 13%.

In the second type of the test (trapezoidal shape), the MPPT sliding mode controller deviates the operating point from the maximum power point about 3%. Hence, the oscillations of magnitudes remain acceptable.

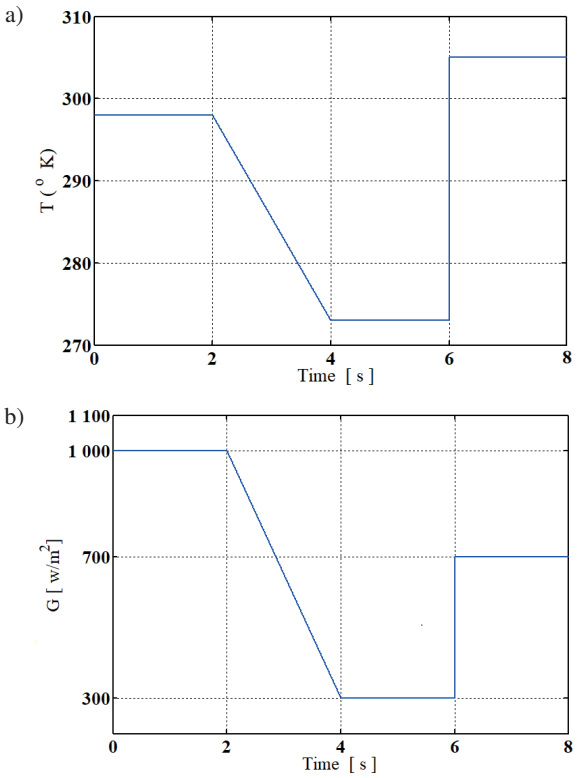

Fig. 7. Change of irradiation and temperature

Here, the inverter in the dq reference plays the same role of a chopper with four switches where the components S_d and S_q represent the duty cycle of the chopper (Fig. 8 g, h).

Thus, the components S_{d_eq} and S_{q_eq} are constant and limited by the normalized components S_{d_n} and S_{q_n} while respecting the principle of the sliding mode (Fig. 8 g, h).

In Fig. 8 g, h, we see that there is a delay in the response of the system. This is due to the convergence mode of the SMC during which the switch remains open $(S_{q\_n} = 0)$ and we see that the sliding surface is reached after 5 ms.

In the case of parametric variations, we took an increase of 50% in stator resistance, 30% in inductance, 200% in inertia, 30% in load, 200% in PV resistance, and 20% in quality factor. The results obtained proved that the variations have an influence on the increase of the response time which is observed on the speed curve (Fig. 8a–e).

Despite the parameters variation, the behaviour of system remains the same as compared to that of fixed parameters. Fig. 8 shows the degradations due to losses of energy.

5. Conclusions

The purpose of this work was initially to contribute to the optimization of photovoltaic pumping system using sliding mode control. The choice of this technique has not been made arbitrarily, but because of the nature of a photovoltaic generator which has highly non-linear characteristics, and the changes in the climatic conditions that depend on it are highly random phenomena.

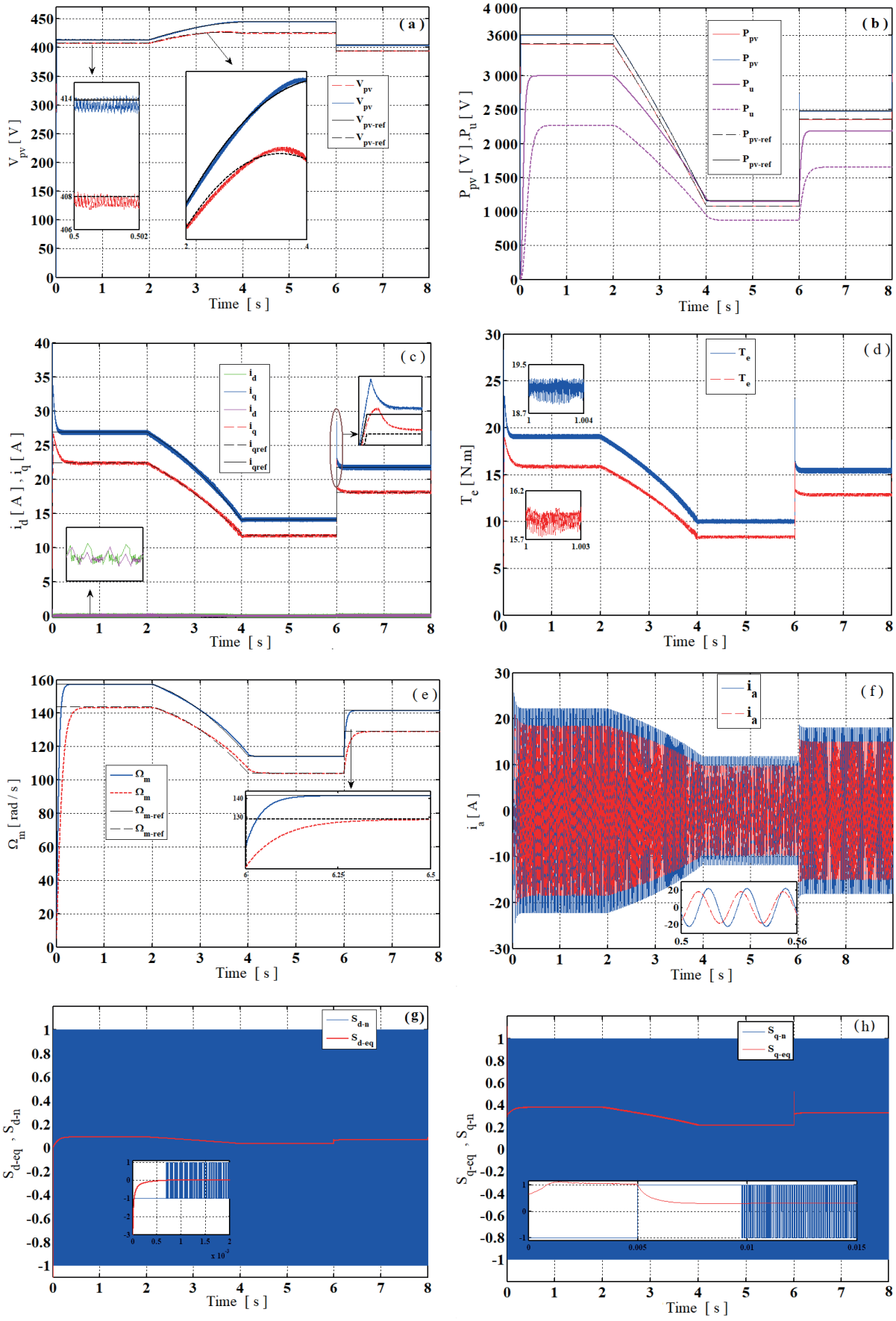

Fig. 8. Simulation results for different sizes of photovoltaic pumping system

The advantage of the developed control is simplicity and minimization of the controllers number to two. One ensures a maximum power extraction the from the PVG and the other ensures good performances under dynamic behaviour conditions using the vector control specification.

The results obtained showed that, whatever the operating conditions, the control system always transfers all the energy produced by the photovoltaic generator to the motor-pump unit. It is important to mention that despite the consideration of the effects of the change in the system parameters; the simulation results showed good dynamic performance of the proposed control system. The Chattering problem appears in the interval where the changes in irradiation and temperature are progressive but remains acceptable.

This regulation presents a simple robust control algorithm that has the advantage of being easily implantable in calculator.

References

[1] K. Benlarbi, L. Mokrani, and M.S. Nait-Said, "A fuzzy global efficiency optimization of a photovoltaic water pumping system", *Solar Energy* 77 (2), 203–216 (2004).

[2] S. Ramirez, J. Hebertt, and R.S. Ortigoza, *Control Design Techniques in Power Electronics Devices*, Springer Science and Business Media, 2006.

[3] R. Chenni et al., "A detailed modeling method for photovoltaic cells", *Energy* 32 (9), 1724–1730 (2007).

[4] M.R. Yaïche and S.M.A. Bekkouche, "Estimation du rayonnement solaire global en Algérie pour différents types de ciel", *Revue des Energies Renouvelables* 13 (4), 683–695 (2010).

[5] V.M. Alves et al., "An effective induction motor control for photovoltaic pumping", *IEEE Transactions on Industrial Electronics* 58 (4), 1162–1170 (2011).

[6] N. Hidouri and L. Sbita, "A new dtc-spmsm drive scheme for pv pumping system", *International Journal of Systems Control* 1 (3), 113–121 (2010).

[7] M. Nabil, S.M. Allam, and E.M. Rashad, "Performance improvement of a photovoltaic pumping system using a synchronous reluctance motor", *Electric Power Components and Systems* 41 (4), 447–464 (2013).

[8] D. Menka, S. Sharma, and R. Saxena, "Solar PV stand-alone water pumping system employing PMSM drive", *Electrical, Electronics and Computer Science* (SCEECS), 2014 IEEE Students' Conference on. IEEE, 2014.

[9] S.R. Shaikh and A.M. Jain, "A high-efficient converter for photovoltaic water pumping system", *Control, Instrumentation, Communication and Computational Technologies* (ICCICCT), 2015 International Conference on. IEEE, 2015.

[10] H. Bouzeria et al., "Fuzzy logic space vector direct torque control of PMSM for photovoltaic water pumping system", *Energy Procedia* 74, 760–771 (2015).

[11] H. Sahraoui et al., "Voltage control of DC-DC buck converter using second order sliding mode control", *Control, Engineering and Information Technology* (CEIT), 2015 3rd International Conference on. IEEE, 2015.

[12] K. Zaouche, A. Talha, and M. Berkouk, "An efficient asymmetric cascaded H-bridge inverter for photovoltaic systems", *Modelling, Identification and Contro*l (ICMIC), 2016 8th International Conference on. IEEE, 2016.

[13] A. Achour et al., "Application of direct torque control to a photovoltaic pumping system with sliding-mode control optimization", *Electric Power Components and Systems* 44 (2), 172–184 (2016).

[14] V. Shankar, A. Kalaiselvan, et al., "Solar PV-Based VFD Fed Permanent Magnet Synchronous Motor for Pumping System", *Artificial Intelligence and Evolutionary Computations in Engineering Systems*, 487–502, Springer, Singapore, 2017.

[15] B. Talbi et al., "A high-performance control scheme for photovoltaic pumping system under sudden irradiance and load changes", *Solar Energy* 159, 353–368 (2018).

[16] S. Dessouky, A. Sobhy, et al., "Performance improvement of a PV-powered induction-motor-driven water pumping system", *Power Systems Conference* (MEPCON), 2016 Eighteenth International Middle East. IEEE, 2016.

[17] B. Sreewirote, N. Akeratana, and P. Chaichan, "Performance and economic analysis of solar water pump system", *Sustainable and Renewable Energy Engineering* (ICSREE), 2017 2nd International Conference. IEEE, 2017.

[18] R. Antonello et al., "Energy-efficient autonomous solar water-pumping system for permanent-magnet synchronous motors", *IEEE Transactions on Industrial Electronics* 64 (1), 43–51 (2017).

[19] E. Deniz, "ANN-based MPPT algorithm for solar PMSM drive system fed by direct-connected PV array", *Neural Computing and Applications* 28 (10), 3061–3072 (2017).

[20] B. Mehimmedetsi and R. Chenni, "Field Oriented Control of PMSM Supplied by Photovoltaic Source", *International Journal of Electrical and Computer Engineering* (*IJECE*) 6 (3), 1233–1247 (2016).

[21] M. Farhat et al., "Variable structure MPP controller for photovoltaic pumping system", *Transactions of the Institute of Measurement and Control* 39 (9), 1283–1292 (2017).

[22] J. Jurasz and J. Mikulik, "Economic and environmental analysis of a hybrid solar, wind and pumped storage hydroelectric energy source: a Polish perspective", *Bull. Pol. Ac.: Tech.* 65 (6), 859–869 (2017).

[23] K. Urbanski, "A new sensorless speed control structure for PMSM using reference model", *Bull. Pol. Ac.: Tech.* 65 (4), 489–496 (2017).

[24] X. Sun et al., "Design and analysis of interior composite-rotor bearingless permanent magnet synchronous motors with two layer permanent magnets", *Bull. Pol. Ac.: Tech.* 65 (6), 833–843 (2017).

[25] J. Yang, M. Dou, and D. Zhao, "Iterative sliding mode observer for sensorless control of five-phase permanent magnet synchronous motor". *Bull. Pol. Ac.: Tech.* 65 (6), 845–857 (2017).

Appendix

Parameters of three phase PMSM motor and PV generator:

$P_n = 3$ kW, $V_n = 230$ V, $I_n = 23$ A, $R_a = 2.83\ \Omega$, $L_s = 2.83$ mH, $p = 4$, $J_m = 0.03$ kg·m^2, $\phi_m = 0.177$ Wb, $k_f = 0.005$ Nm·s/rad, $C_{pv} = 3300\ \mu$F, $f_H = 15$ kHz, $P_{pv} = 3.6$ kW, $N_s = 12$, $N_p = 2$.

Parameters of sliding mode:

$k_d = 0.25$, $k_q = 200$.